Lab on a Chip

Check for updates

Acoustically modulated biomechanical stimulation for human cartilage tissue engineering†‡

Umesh S. Jonnalagadda, [iD][a] Martyn Hill, [iD][a] Walid Messaoudi,[a] Richard B. Cook,[a] Richard O. C. Oreffo, [iD][b] Peter Glynne-Jones [iD]*[a] and Rahul S. Tare [iD]*[ab]

Bioacoustofluidics can be used to trap and levitate cells within a fluid channel, thereby facilitating scaffold-free tissue engineering in a 3D environment. In the present study, we have designed and characterised an acoustofluidic bioreactor platform, which applies acoustic forces to mechanically stimulate aggregates of human articular chondrocytes in long-term levitated culture. By varying the acoustic parameters (amplitude, frequency sweep, and sweep repetition rate), cells were stimulated by oscillatory fluid shear stresses, which were dynamically modulated at different sweep repetition rates (1–50 Hz). Furthermore, in combination with appropriate biochemical cues, the acoustic stimulation was tuned to engineer human cartilage constructs with structural and mechanical properties comparable to those of native human cartilage, as assessed by immunohistology and nano-indentation, respectively. The findings of this study demonstrate the capability of acoustofluidics to provide a tuneable biomechanical force for the culture and development of hyaline-like human cartilage constructs *in vitro*.

Articular cartilage is a highly specialized form of hyaline cartilage that functions as a low-friction surface to allow for smooth articulation of the joints.[1] Given the avascular nature of the tissue and low mitotic activity of the resident chondrocytes, adult articular cartilage exhibits a limited capacity for self-repair. There are currently no effective pharmacological agents to promote comprehensive healing of articular cartilage defects and while surgical treatments, such as autologous chondrocyte implantation and microfracture, provide temporary relief to patients, these approaches are unable to restore the functionality of the damaged tissue over the long term.[2,3] To this end, tissue engineering has been employed to generate functionally relevant, hyaline-like cartilage grafts.

Tissue engineering aims to repair, replace, maintain, or enhance native host tissue.[4,5] These goals are typically accomplished through the *in vitro* culture of cells, supported by the application of appropriate biochemical/biomechanical cues, scaffolds/biomaterials, and bioreactor/culture systems to generate 3-dimensional (3D) tissue constructs for the eventual implantation into patients. To date, several groups have shown promising results in developing skeletal tissue structures, such as bone[6–11] and cartilage.[6,10,12–16] In the field of cartilage bioengineering, research has included the application of a variety of modalities, including pellet culture,[17] deposition printers,[10,18–20] micro-scale bioreactors[21] and stackable cell sheets.[22,23]

Literature has highlighted the importance of the physiochemical environment in promoting robust cartilage generation.[24,25] Mechanical stimulation using hydrostatic loads and cell stretching, among other forces, have been applied to activate mechanotransduction pathways and promote chondrogenesis in cells.[26,27] Dynamic stimulation (*e.g.* cyclic shear or dynamic compression) of the cells has been shown to result in the generation of more robust cartilage, compared to stimulation of cells with static forces.[26] Furthermore, mechanical stimulation of chondrocytes results in the secretion of parathyroid hormone-related protein (PTHrP), a chemical factor that has been found to aid chondrogenesis and reduce hypertrophy.[28–30] Thus, there is clear evidence that biomechanical stimulation of chondrocytes promotes chondrogenesis.

In recent years, cell-environment responses and phenotypic changes have been investigated in the field of bioacoustofluidics using ultrasonic standing wave fields. Ultrasonic standing wave fields, or acoustic traps, have been applied to induce patterning, alignment, and clustering of cells using either bulk acoustic waves (BAWs),[31–35] or surface

[a] *Mechanical Engineering, Faculty of Engineering and the Environment, University of Southampton, Southampton SO17 1 BJ, UK.*
E-mail: P.Glynne-Jones@soton.ac.uk; Tel: +44 (0)23 8059 5769
[b] *Centre for Human Development, Stem Cells and Regeneration, Institute of Developmental Sciences, Faculty of Medicine, University of Southampton, Southampton SO16 6YD, UK.* E-mail: R.Tare@soton.ac.uk;
Tel: +44 (0)23 8120 5257

acoustic waves (SAWs)[36,37] within micro-channels. Recent literature has described a number of configurations of both SAW[37,38] and BAW[14,32] based traps for cell manipulation, and preliminary findings have shown their ability to engineer functional hepatocyte and neuronal aggregates using scaffold-based and scaffold-free methodologies.[39,40]

BAW manipulation typically occurs within a layered resonator,[41] where a piezoelectric transducer is coupled to a chamber. The transducer creates a standing wave field within the fluid space of the chamber, within which an energy gradient subjects cells to acoustic radiation forces. As cells are introduced into the wave field, primary radiation forces direct the cells to a region of low acoustic potential energy, the pressure node. Variations of acoustic velocity amplitude within the pressure node,[42] along with intercellular attraction due to Bjerknes forces,[43] draw the cells into a levitated aggregate.

In the current study, we have used an acoustic trap to aggregate cells and by modifying the ultrasonic field we have generated time-varying radiation forces and drag forces on the cell aggregates. A number of groups have suggested that similar acoustically generated forces can affect cells and matrix proteins within the field.[14,31,44,45] The repeated displacement of the cells introduces mechanical stimulation in the form of fluid shear stress and this has the potential to alter the development of cartilage tissue within a scaffold-free environment. To date, however, investigation of scaffold-free tissue culture via bioacoustofluidics has been limited and little is known concerning the exploitation of the acoustic environment to maximise the potential of this approach.

Previously, we have demonstrated the potential of acoustic trapping for scaffold-free development of hyaline-like cartilage constructs,[14] by means of the long-term levitation of chondrocytes within an acoustofluidic bioreactor coupled with perfusion-based media exchange. The acoustic trap overcame some of the issues associated with conventional static pellet culture, specifically the lack of mechanical stimulation, inefficient oxygen diffusion and suboptimal metabolite mass transfer rates that adversely affect the scale-up, quality (i.e. formation of fibrous versus hyaline cartilage) and biomechanical properties of the cartilaginous constructs.[46] However, the contribution of different aspects of the acoustic environment to enhanced cartilage production remained unclear, and the closed fluidic loop had significant problems relating to bubble generation.

Here, we present a second-generation open design (i.e. a design with a free fluid surface adjacent to each resonant cavity) that has the advantages of immunity from bubble buildup, easy cell injection, parallelized throughput, and the potential for scaling to larger construct sizes. Crucially, we identify sources of mechanical stimulation created in our bioreactor, and demonstrate that these forces can be electronically modulated to produce human cartilage with improved physical properties. The combination of this acoustically induced mechanical stimulation and the growth factor PTHrP has been investigated and found to promote robust cartilage development.

Results

An open layered resonator configuration was adopted as shown in Fig. 1. The device comprises of a number of acoustically resonant cavities which are actuated by piezoelectric transducers situated below each one. Cells are introduced into the open-sided cavities using a gel-loading pipette. Acoustic levitation holds cells at the pressure node of the acoustic resonances and also brings the cells together laterally into a number of discrete aggregates within the resonator. Cells are drawn to the areas of high kinetic energy density modelled in Fig. 1C (more detailed information on the acoustic design can be found in the ESI†). The open design enables free exchange of gases to the environment (alleviating the problems with bubbles found in our previous work). Characterization of the resonators, including the reproducibility of their assembly, is discussed in the ESI† (S1).

The acousto-mechanical culture environment

Sweeping over a range of frequencies, as opposed to driving at a single frequency, has been used in acoustofluidics to create a time-averaged field containing contributions from a number of resonant modes,[47–49] to effect particle transport[50] or simply to ensure a mode was excited even if its precise centre frequency was unknown.[14] In this work however, frequency sweeping is found to modify the mechanical environment experienced by the cell constructs by dynamically moving them over the course of a sweep. It is shown that by making small variations to the electrical driving frequency around the acoustic resonance the acoustic force field changes, resulting in displacement of the aggregation positions of the cells laterally. Thus, by periodically varying this frequency (using a linear frequency sweep: variations of ±100 kHz at sweep repetition rates of up to 50 Hz), the aggregates vibrate backwards and forwards, inducing fluidic shear and deformational stress on the cell aggregates. In this manuscript, we use the term sweep repetition rate to denote how often the sequence of applied frequencies is cycled through, exploring a range of 1–50 Hz. This corresponds to the observable frequency of lateral vibration of the aggregates. It is important to note that the cells will be exposed to both the lateral, cyclic oscillations from the frequency sweep and to constant fluid flux as a result of acoustic streaming within the wave field, but the magnitude of the stresses due to the movement of the aggregate is found to be more than an order of magnitude higher than the streaming-induced stresses. As the cells are trapped at the pressure node of a standing wave, they do not experience pressure variations from the acoustic field, however as this is also the velocity antinode, density difference between the cells and the media leads to MHz frequency shear on the cells due to the acoustic excitation itself. This does not change significantly under the different driving conditions, hence is considered a constant throughout the different cell culture investigations. We also note that studies over shorter timescales have shown
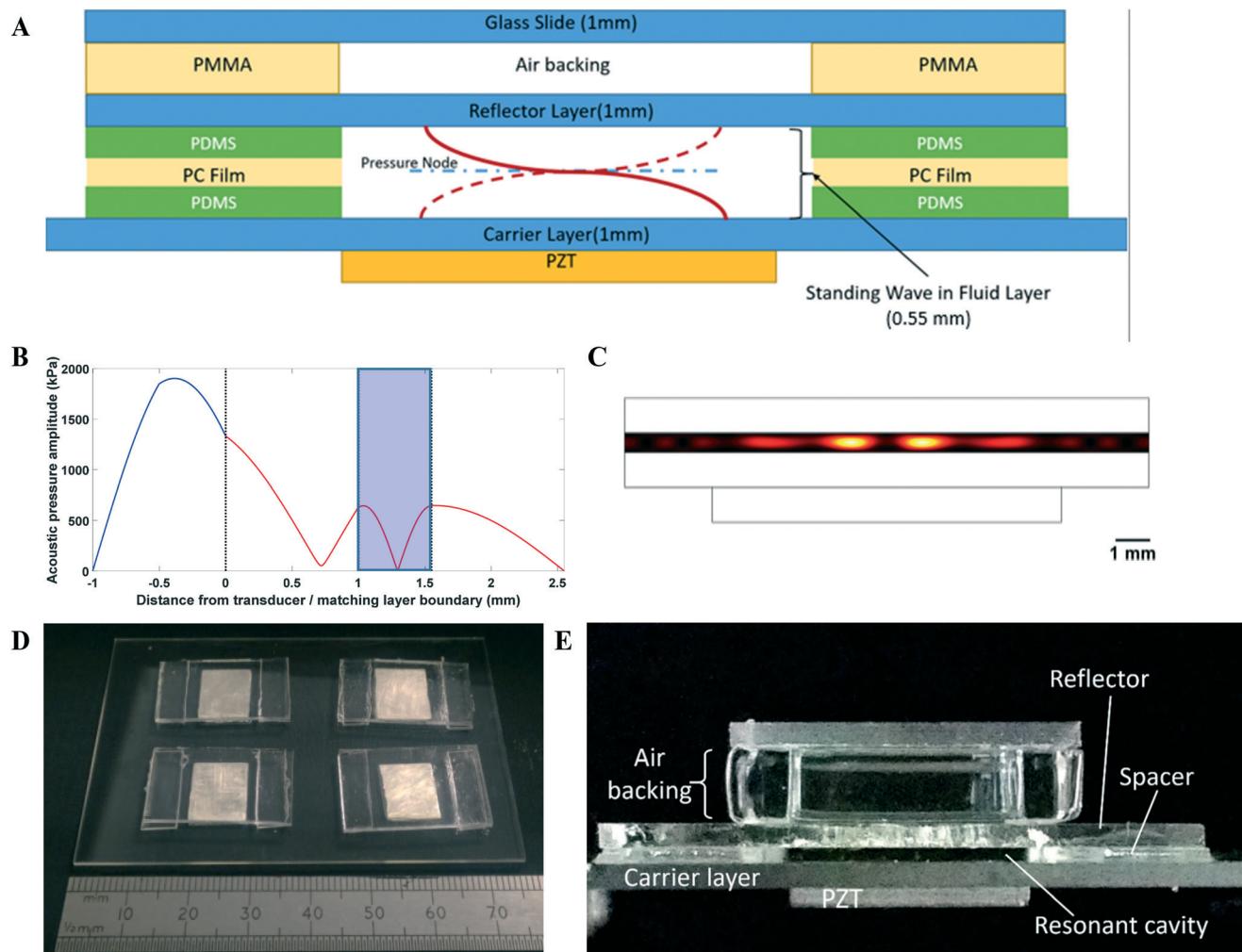
Fig. 1 Bioreactor design and modelling. (A) Schematic diagram detailing resonator design and the dimensions of each layer. (B) A 1-dimensional model was used to confirm cavity resonance frequency and the presence of a pressure node near the centre of the fluid cavity (blue region) for the desired resonator configuration. (C) The transfer impedance model was further validated with a FE model to determine the kinetic energy distribution at resonance, in order to better predict the energy distribution within the pressure node and where the cells are likely to levitate. (D) Angled top view of assembled plate to detail arrangement of multiple resonators on a single double-width glass slide. (E) Side view of assembled resonator, labelled to indicate position of PZT, spacers, carrier and reflector layers. The open sides of the resonant cavity allow for medium exchange within the cavity and alleviate problems with bubble formation experienced with previous closed resonator designs.

minimal bio-effect from the MHz shear stresses induced by levitation fields of comparable magnitude.[51]

As the frequency varies during each sweep, both the lateral acoustic forces and associated trapping positions change, so the relationship between the input frequency and the construct response would not be expected to be a linear one. Essentially, the aggregate is sequentially attracted to a number of trapping locations during the period of a sweep. Thus, it is observed that the construct movement and the associated mechanical stresses have frequency components of a higher order than the sweep repetition rate. The magnitude of the shear stresses on the cells varies with both the sweep repetition rate and the amplitude of the driving waveform as discussed below.

To assess the quality of the hyaline-like cartilage produced in the bioreactor, the chondrocytes were cultured for an ex-

tended period to allow for maturation of the cells and expression of key chondrogenic markers.[52,53] A culture period of 21 days under continuous acoustic excitation within the bioreactor was therefore used throughout the work. In the initial phase of cell culture within the bioreactor (typically around 14 days), aggregates were levitated with no contact with the resonator walls, and we hypothesize that the primary source of stress on the cells at this time is from the lateral oscillations. During the culture period beyond 14 days, the aggregates typically grew to a point at which the aggregates were in contact with the resonator walls and ceased to move freely. Throughout this phase the acoustic forces are more likely to induce deformational stresses, however we only quantify the fluid-shear derived forces in this paper.

Perfusion and acoustic streaming flows. Acoustic streaming is the mean flow induced in a fluid due to absorption of
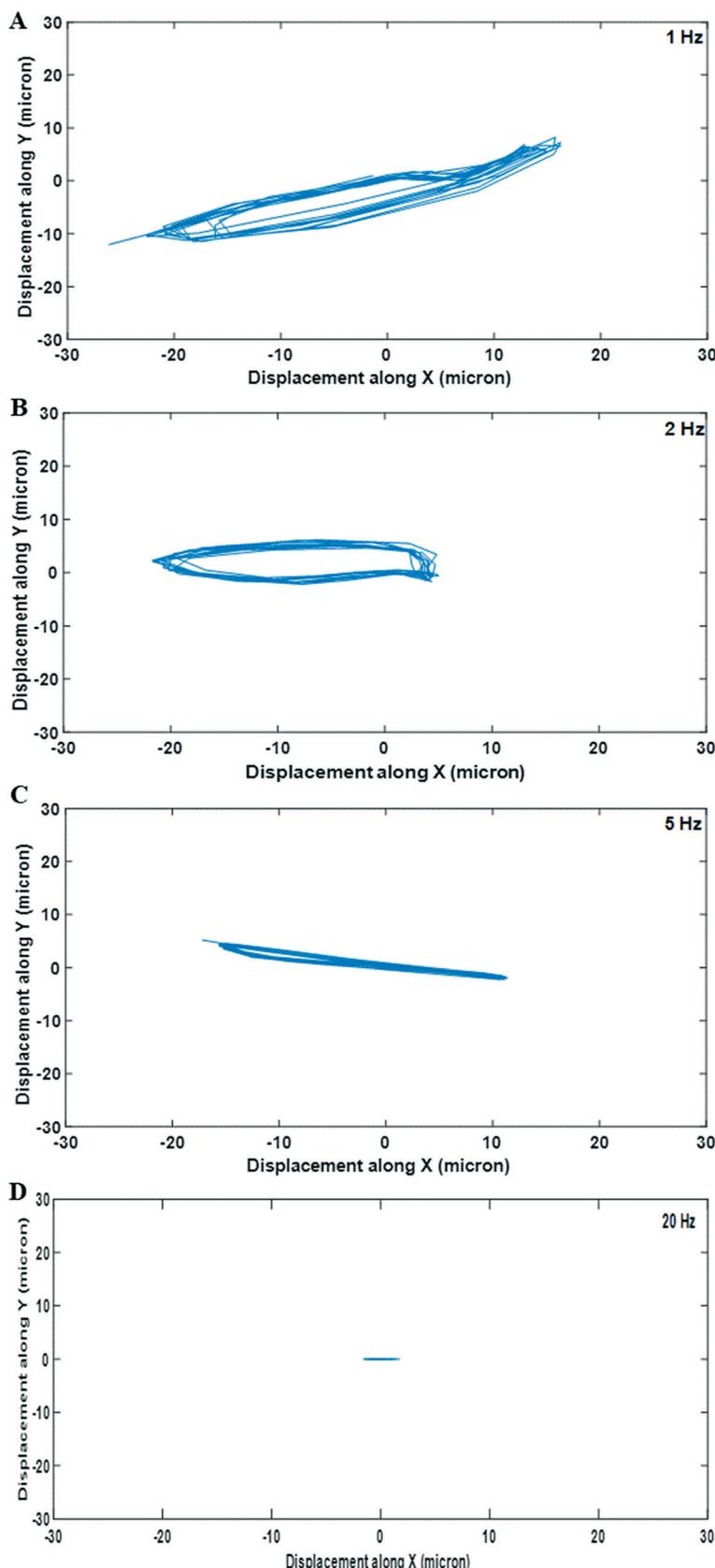
Fig. 2 Measuring cell displacement during acoustic stimulation to calculate induced stresses. Cell aggregates were subjected to varying cyclic stimulation regimes (A: 1 Hz; B: 2 Hz; C: 5 Hz; D: 20 Hz). The acoustic forces drag the aggregates through the fluid along the paths shown here. This data is later fed into a model to calculate the shear stresses experienced by the aggregates as they move. The displacement amplitude and path were found to vary with the sweep repetition rate (values inset in each graph). The sweep range was 200 kHz, voltage amplitude 10 V_{pp}.

acoustic energy.[54,55] In the present study, boundary driven transducer-plane streaming is observed, which results from acoustic energy dissipated at the device walls.[56,57] Motion of the media due to acoustic streaming, coupled with block media changes, provide the perfusion for the cell aggregates in contrast to the previously reported system[14] which relied on the pumping of media. Streaming velocities are expected to be independent of the sweep repetition rate,[58] and in our system are measured to be of the order of 2 μm s^{-1}. The shear stresses on the cell aggregates resulting from these streaming flows are of the order of 13 μPa. These continuous stresses will be applied to the aggregates in addition to the larger time-varying stresses derived from the periodic lateral movement discussed below. It is important to note that the average acoustic energy entering the system is independent of the sweep repetition rate, hence other acoustic energy effects on cells (such as heating) will also be independent of this.

Quantifying and modulating aggregate displacement and fluidic shear stresses. To quantify how the acoustic driving parameters modulate fluidic shear stresses, the paths traced out by the cell aggregates in levitation were imaged. Fig. 2 shows example paths. It was observed that the sweep repetition rate affected the shape of the path followed by the cell aggregate (Fig. 2), and the size of the area traced out. Higher sweep repetition rates displayed reduced lateral displacement of the cells, with 20 Hz displaying virtually no measurable displacement. We deduce that for the parameters explored, the aggregates are in dynamic motion, limited by viscous drag. Essentially, at higher rates the aggregates have less time to move significantly before being redirected towards another location.

In the ESI† (S2), we describe a finite element model used to estimate the fluidic shear stresses induced by the experimentally observed aggregate motion. The time-varying shear stress is plotted in Fig. 3A, and presents a steady, periodic waveform. Given the cyclic nature of the stress and the complex two-dimensional pattern of the cell aggregate movement we choose to extract the peak-to-peak value of the stress waveform for subsequent comparison. The relationship between sweep repetition rate and shear stress is presented in Fig. 3B, which shows relatively high shear stresses between 2 and 10 Hz, but with significantly reduced stresses at the higher sweep repetition rates of 20 and 50 Hz. Further detailed examination of the role of driving voltage and repeatability (at 2 Hz) is shown in Fig. 3C – increased voltage leads to increased shear stresses, related to the expected squared dependence of acoustic forces on driving voltage.

As a result, control of both the sweep repetition rate and the driving voltage enable the system to be programmed to deliver a specific frequency and amplitude of mechanical stimulation to the cells over the course of the culture period. In order to investigate the effect of sweep repetition rate on cartilage formation, two frequencies were chosen. A lower frequency, high peak stress (example of 2 Hz), which is within the range of frequencies often chosen for conventional dynamic compression,[59,60] and a higher frequency, low peak
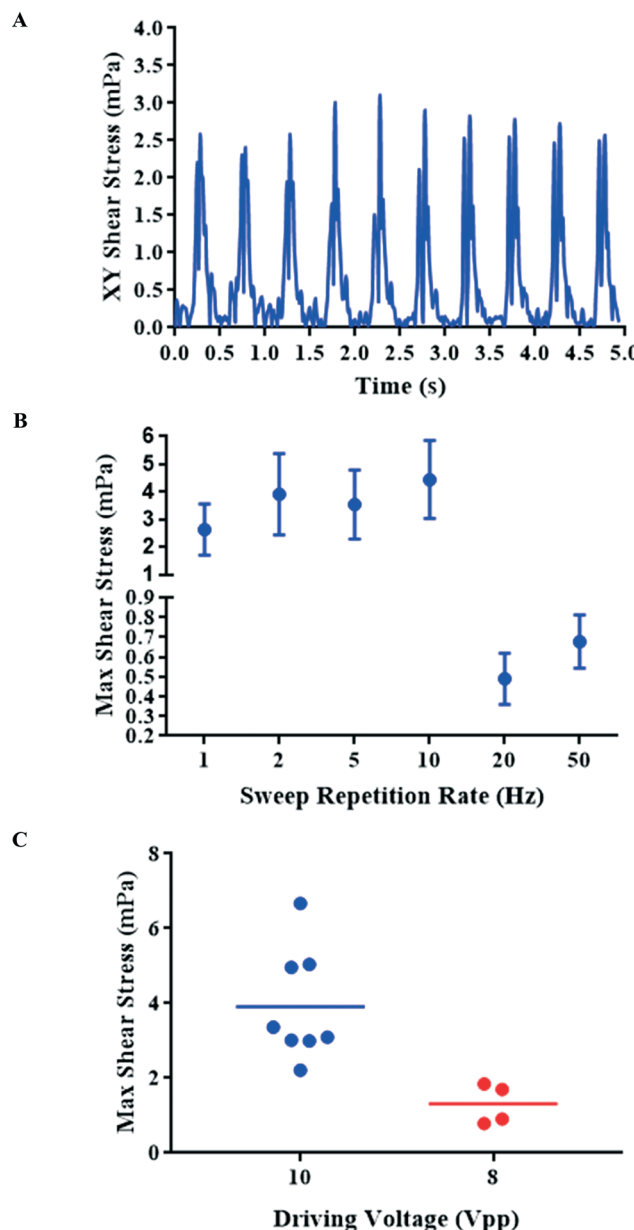
Fig. 3 Shear stress profiles of cells under different driving parameters: fluidic shear was calculated by applying measured aggregate displacements to an FE model. (A) The magnitude of the fluidic shear experienced by the aggregate shown in Fig. 2B (2 Hz sweep repetition rate). (B) Maximum shear stresses calculated for different sweep repetition rates and a driving voltage of 10 V_{pp} (n = 7–8, data shown as mean ± SD). (C) Maximum shear stress at different driving voltages (n = 4 for 8 V_{pp}, n = 8 for 10 V_{pp}) showing mean as a horizontal bar. The sweep frequency range is 200 kHz in all cases.

stress (example of 50 Hz), which corresponds to the frequency used in our earlier study.[14]

Biological response to physicochemical environment within acoustic trap

The role of the physicochemical environment within the acoustic trap in stimulating cartilage development was

assessed at different sweep repetition rates at constant drive voltage. The mechanical stimulation regime that promoted cartilage formation was then supplemented with the growth factor, PTHrP, to examine whether this provided additional chemical cues in combination with mechanical stimulation for improved hyaline-like cartilage formation. Considering the qualitative nature of histochemical staining, semi-quantification of the staining of 50 Hz, 2 Hz, and 2 Hz + PTHrP constructs was performed by image segmentation (Fig. S7†) to approximate the matrix staining fraction relative to the total tissue section area. As the desired tissue is hyaline-like cartilage, the tissue quality was evaluated by the matrix composition of proteoglycans (Alcian blue staining) and collagen Type-II immunostaining. The relative staining

fractions for these markers were then compared against collagen Type-I (marker for fibrocartilage) and collagen Type-X (marker for hypertrophic cartilage).

21 day culture of human articular chondrocyte (HAC) aggregates in presence of varying sweep repetition rates. HAC aggregates were cultured for 21 days in the acoustic traps using either a sweep repetition rate of 50 Hz (Fig. 4A, Fig. S2 and S8A†) or 2 Hz (Fig. 4B, Fig. S3 and S8B†) and the resulting 3-D tissue constructs were harvested for histological and immunohistochemical analyses to assess cartilage formation.

Day-21 constructs generated in the bioreactor in response to a sweep repetition rate of 50 Hz (Fig. 4A, Fig. S4 and S8A†) were compact in size (cross-sectional area of 0.343 mm^2 ±
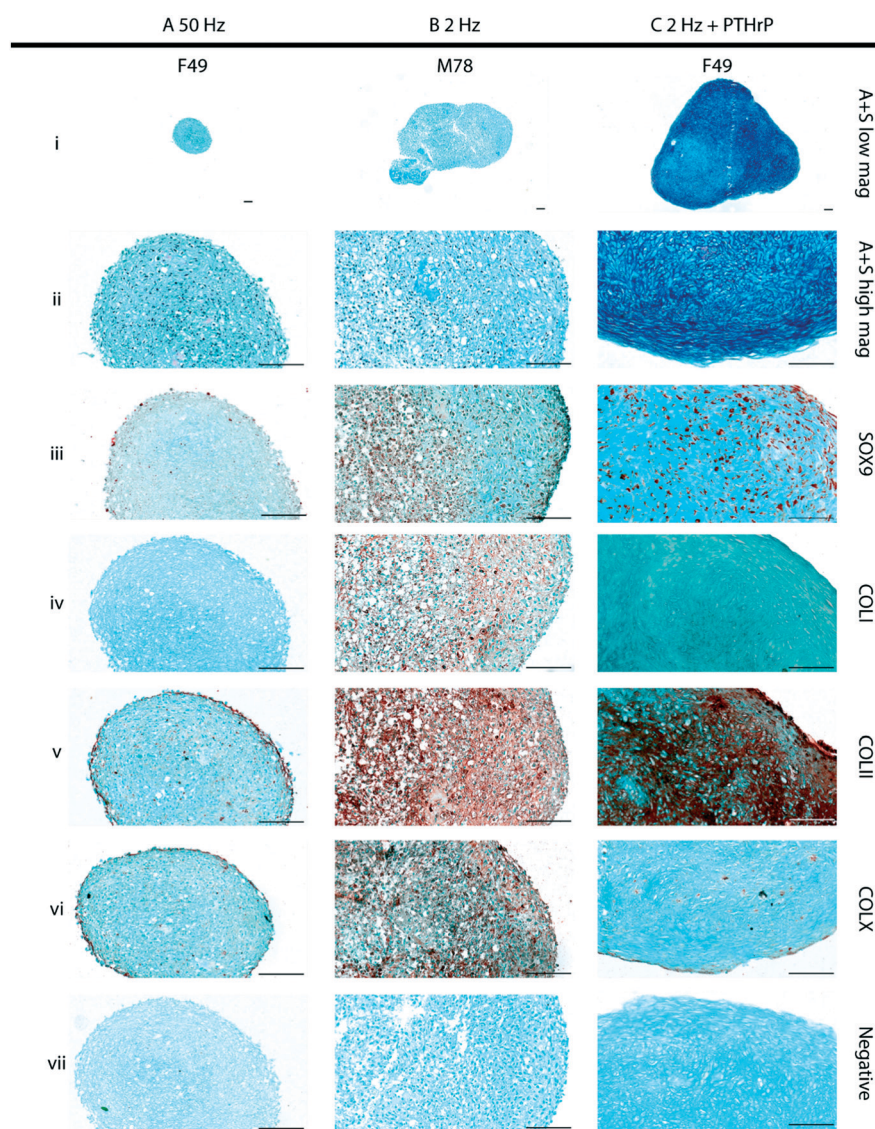
Fig. 4 Histological analyses of cartilage constructs engineered under different physicochemical environments. 21 day cartilage constructs engineered in resonators at (A) 50 Hz, (B) 2 Hz and (C) 2 Hz in combination with 10 ng ml^{-1} PTHrP supplementation. Alcian blue + Sirius red (A + S, i and ii) staining was performed on sections of the cartilage constructs to assess the histological structure, while formation of hyaline-like cartilage was confirmed by robust immunostaining for SOX-9 (iii) and Type II collagen (COLII, v), and negligible immunostaining for collagens Type I (COLI, iv) and Type X (COLX, vi). No staining was observed in the negative controls (omission of the primary antisera, vii) included in all immunostaining procedures. Tissue sections were selected from a representative set of (A) three patients and (B and C) four patients. Scale bars = 100 μm.

0.235 across all patients) and appeared as aggregates of cells held together by extracellular matrix, composed largely of proteoglycans evidenced by Alcian blue staining (Fig. 4Ai and ii, Fig. S2i and ii and S8Ai†). The constructs exhibited minimal expression of the chondrogenic proteins, namely SOX-9 (Fig. 4Aiii, Fig. S2iii and S8Aii†) and Type-II collagen (COLII) (Fig. 4Av, Fig. S2v and S8Aiv†), coupled with minimal immunostaining for collagens Type-I (COLI) and Type-X (COL X) (Fig. 4Aiv and vi; Fig. S2iv and vi and S8Aiii and v,† respectively).

In contrast, day 21 constructs generated in the bioreactor in response to a sweep repetition rate of 2 Hz (Fig. 4B, Fig. S3 and S8B†) were consistently larger in size (cross-sectional area of 0.878 mm^2 ± 0.353 across all patients). Most cells in the cartilaginous constructs were located within distinct lacunae embedded in the Alcian blue-stained, proteoglycan-rich extracellular matrix (Fig. 4Bi and ii). Moreover, robust expression for SOX-9 and COLII were observed in the cells and the surrounding extracellular matrix, respectively (Fig. 4Biii and v; Fig. S3iii and v and S8Bii and iv†). However, it was possible to detect distinct immunostaining for COLI and COLX in the extracellular matrix of the cartilaginous constructs (Fig. 4Biv and vi; Fig. S3iv and vi and S8Biii and v†).

21 day culture of HAC aggregates in the bioreactor supplemented with PTHrP. To assess the possibility of further enhancing cartilage formation in the constructs, chondrocyte aggregates stimulated with a sweep repetition rate regime of 2 Hz for three weeks in the bioreactor were cultured in chondrogenic medium supplemented with PTHrP from day 10 to day 21 (*i.e.* 2 Hz + PTHrP regime). Day-21 constructs generated using these culture conditions (Fig. 4C, Fig. S4 and S8C†) were appreciably larger in size (cross-sectional area of 1.45 mm^2 ± 0.804 across all patients) compared to constructs generated in response to sweep repetition rates of 50 Hz and 2 Hz without the supplementation of PTHrP. The tissue generated within the constructs was reminiscent of native hyaline cartilage and was composed of numerous chondrocytes, characterized by the expression of SOX-9, located within distinct lacunae embedded in dense extracellular matrix constituted by Alcian blue-stained proteoglycans and abundant COLII (Fig. 4Ci–iii and v; Fig. S4i–iii and v and S8C i–ii and iv†). Furthermore, expression of COLI was markedly reduced in the cartilaginous constructs and restricted to the peripheral layer of the constructs (Fig. 4Civ; Fig. S4iv and S8Ciii†). Due to the inhibitory effect of PTHrP on chondrocyte hypertrophy, negligible expression of COLX was observed in the extracellular matrix of the cartilaginous constructs (Fig. 4Cvi; Fig. S4vi and S8Cv†). This, coupled with the marked absence of the two hypertrophic markers, namely osteopontin (OPN) and alkaline phosphatase (ALP), confirmed that the culture regime prevented terminal differentiation of the chondrocytes within the hyaline-like cartilage constructs (Fig. S5†). Nano-indentation showed that the mean (± SD) elastic modulus (187 ± 23 kPa) of the human cartilage constructs engineered using the 2 Hz + PTHrP regime was comparable to the average elastic modulus (200 ± 63 kPa) of native human articular cartilage (Fig. 5).

Discussion

In the present study, we have designed a novel acoustofluidic bioreactor system for the culture of HAC aggregates in levitation to generate 3D, hyaline-like cartilage. We have investigated and quantified how the fluidic shear stresses produced by the bioreactor could be modulated electronically, and assessed resulting differences in the quality of cartilage formation in the engineered constructs. We have shown that the ability to modulate the stresses provides the possibility of tuning the system to promote better cartilage formation.

The influence of the acoustically induced forces on cell and fluid displacement was quantified by particle tracking, following which computational modelling tools were used to estimate the magnitude of the fluid shear stress on the cells. Acoustic streaming allowed for nutrient exchange around the developing tissue in the place of bulk perfusion used in the first-generation acoustofluidic bioreactor.[14]

The stimulation created by oscillating the cell agglomerate laterally at a rate determined by the sweep repetition rate has a number of key advantages. Acoustic stimulation of cells has been reported to be complex and multifaceted, resulting in the repair, proliferation, and differentiation of numerous cell types.[61–63] It is a key feature of our method that the acoustic energy absorbed by the system (and hence any heating) is independent of the sweep repetition rate, providing a means to isolate the mechanical component of the resulting stimulation, as well as tailor it for specific goals. The contact-free nature of the stimulation is in contrast to contact-based methods which can reduce the surface area of the aggregate available for perfusion.[64] While it would be possible to design a bubble-resistant open system with shear induced by bulk perfusion, the current design allows for electronically controllable oscillatory shear at frequencies that would be more difficult to achieve in a bulk flow system. In addition, bulk perfusion requires that the levitated construct be held against
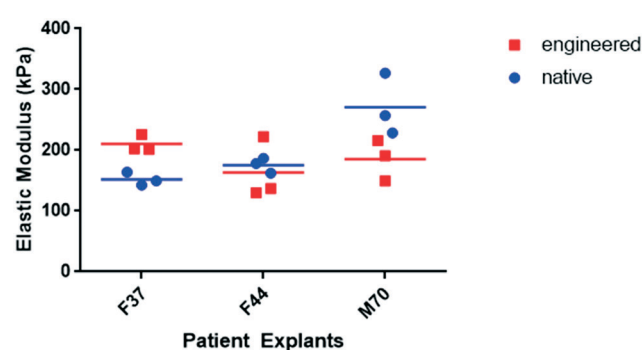
Fig. 5 Young's modulus of native human articular cartilage and 21 day cartilage constructs engineered in resonators at 2 Hz in combination with 10 ng ml^{-1} PTHrP. The elastic modulus of the engineered constructs was compared against native human articular cartilage using nano-indentation. Data acquired from three indentation points were used to determine the mean values for Young's/elastic moduli of engineered and native articular cartilage. Figure shows data distribution and the mean values as horizontal bars; *n* = 3 patients, namely F37, F44 and M70.

the perfusion flow by the lateral acoustic radiation forces, limiting the magnitude of achievable flows.

The bio-effects of modulating the acoustic field on cartilage generation were determined by comprehensive immunohistological analyses of the cartilage constructs, generated as a result of 3-D, scaffold-free culture of HACs in the acoustofluidic bioreactor over a period of 21 days. This study found that a higher sweep rate (50 Hz), which produces lower shear stresses, resulted in sub-optimal formation of hyaline-like cartilage. In contrast, a 2 Hz regime resulted in the generation of cartilaginous constructs exhibiting regions of hyaline-like structure, characterized by robust SOX-9 and Type II collagen expression. However, the constructs were also characterized by the conspicuous presence of collagens Type I and Type X, normally expressed in fibrous and hypertrophic cartilage, respectively. This suggested that, although mechanical stimulation as a result of application of the sweep repetition rate of 2 Hz elicited a favorable chondrogenic response from the cells, further parameter optimization was necessary to promote the formation of robust hyaline-like cartilage and to minimize hypertrophy. Our previous study[14] demonstrated robust cell viability and negligible cell necrosis in day-21 cartilage constructs generated using the acoustofluidic bioreactor. Bazou et al.[51] also showed that the acoustic energy density required for levitation had no significant impact on hepatocyte viability over a period of hours, a conclusion supported by a separate study.[65] In this study, we have not assessed cell viability directly; it can be inferred that in constructs exhibiting robust cartilage production, cell viability will be good, however in constructs with suboptimal cartilage production we do not have data to point to the cause.

To improve cartilage formation, in addition to manipulating the mechanical environment, culture of the HAC aggregates within the acoustic field was investigated in the presence of PTHrP, a growth factor with defined roles in promoting chondrogenesis and inhibiting hypertrophy, especially in presence of mechanical stimulation.[28–30] Notably, 21 day constructs generated in the bioreactor in chondrogenic media supplemented with PTHrP, using a sweep repetition rate of 2 Hz were: i) appreciably larger in size, ii) exhibited distinct hyaline-like cartilage structure, iii) demonstrated robust expression of SOX-9 and Type II collagen, and, importantly, iv) displayed negligible expression of collagens Type I and Type X. Additionally, mechanical analysis of the cartilage tissue using nano-indentation showed the engineered human cartilage constructs to have stiffness similar to that of native human cartilage tissue.

With regard to literature concerning biomechanical stimulation, Schatti et al. implemented a parametric analysis study of compressive loading on chondrocytes and found that the rate of stimulation and magnitude of force affected the matrix composition of the tissue.[66] Correspondingly, we have examined and quantified the biomechanical stimulation applied by the acoustically derived periodic fluidic shear to aggregates, and shown how it can be modulated by varying the acoustic parameters. There are likely to be other inter-acting forces at play during the culture period, and further characterization of the interaction between the acoustic environment and the cells will be carried out in the future work, along with assessment of changes in chondrogenic gene expression in response to the acoustic environment. In summary our findings demonstrate the capability of acoustofluidics as a tuneable biomechanical force for the culture and development of hyaline-like human cartilage constructs in vitro and provide a new platform to investigate scaffold-free cartilage tissue engineering.

Materials and methods

All chemicals were purchased from Sigma-Aldrich UK and Invitrogen UK, unless stated otherwise.

Bioreactor design

A schematic of the resonator design is depicted in Fig. 1A. To fabricate the resonators, double-width glass slides (Corning, 75 × 50 × 1 mm) and standard microscope slides (Corning, 75 × 25 × 1 mm) were acid cleaned in a 6 M HCl solution for 3 hours. Double-width slides were washed in distilled water before adhesion to the piezoelectric transducers (Ferroperm PZ26, Kvistgaard, Denmark; 10 × 12 × 1 mm) with epoxy (Epoxy 353, Epotek, Billerica, MA, USA) at 80 °C for 1 hour. Four transducers were coupled to each double-width slide, which functioned as the carrier layer (Fig. 1D). Microscope slides were cut to 13 × 25 × 1 mm, which functioned as the reflector layer for the resonators. Polycarbonate film (500 micron Lexan, Cadillac Plastics) functioned as a spacer between the carrier and reflector and was coupled using PDMS (Dow Chemical Sylgard 182 1 : 10 curing agent : monomer). Fig. 1E depicts the assembled resonator. A laser cut poly(methyl methacrylate) (PMMA) spacer served to create an air cavity behind the reflector in conjunction with a second piece of glass of the same size as the reflector to maintain an air backing to the reflector layer. This air layer was important as it maintained the acoustic boundary conditions needed to excite the required half-wave resonance; without the seal provided by the spacer and the top glass layer, condensation of medium on top of the reflector was liable to change the boundary impedance. Polypropylene (5 mm, Aquarius Plastics) was cut to shape using a laser cutter and grooves were introduced into the top and bottom sheets using a micro-mill to fit the double-width glass slides and create a sealed environment to maintain a sterile culture environment (Fig. S6†).

Acoustic modelling and characterization

A 1D transfer impedance model[67] in MATLAB was used to guide the design and predict the acoustic pressure node configuration and resonant frequency of the system (Table 1 for summary of layer dimensions and sound velocities). The half-wave resonance was predicted at 1.49 MHz (Fig. 1B) and, experimentally, the resonant frequency of the various resonators was measured at 1.47–1.53 MHz from the electrical impedance spectra.

Table 1 Table of parameters for 1D transfer impedance model and 2D FEM of resonator

Parameter name	Value/expression	Units
Transfer impedance model parameters		
Fluid layer thickness	550	µm
Carrier/reflector layer thickness	1000	µm
Piezoelectric transducer thickness	1000	µm
Adhesive layer thickness	1	µm
Density of carrier and reflector layer material	2500	kg m^{-3}
Density of fluid layer material	1000	kg m^{-3}
Density of adhesive layer	1080	kg m^{-3}
Speed of sound through adhesive layer	2640	m s^{-1}
Speed of sound through carrier and reflector layer	5872	m s^{-1}
Speed of sound through fluid layer	1540	m s^{-1}
Driving voltage	10	V$_{pp}$
Q-factor of layers	100	
COMSOL Model Parameters		
Fluid layer thickness	550	µm
Carrier/reflector/PZT dimensions (width × thickness)	10 × 1	mm
Speed of sound in fluid layer	1540	m s^{-1}

The voltage drop method was used to quantify the acoustic pressure generated within the resonators[68] (Fig. S1D†). A 2D finite element model based in "COMSOL multiphysics" was used to produce Fig. 1C. The model included piezoelectric coupling and pressure acoustics within the fluid layer, with sufficient mesh density that the fluid layer mesh was 16 elements thick (Table 1 for resonator model details). The acoustic radiation force was calculated using the Gor'kov equation[69] across a range of frequencies, enabling the resonant frequency to be identified.

An additional COMSOL finite element model was created to calculate the shear stress on a cell aggregate during levitation at a given sweep repetition rate. The lateral movement of cell aggregates was monitored using time lapse imaging at various driving voltages and sweep repetition rates. 16 frames were acquired for each frequency sweep, to ensure sufficient sampling (i.e. the frame rate for the 1 Hz sweep was 16 fps and 800 fps for 50 Hz). Sampling continued until 10 such cycles had been captured. The resulting time-lapse data was analyzed to track the path followed by the aggregates. For the lower frequency regimes, the displacement was estimated using image cross correlation. Pixel quantization error rendered this approach unreliable for the high frequency, low displacement frequency sweep rates of 20 and 50 Hz. In these cases velocities were estimated using particle image velocimetry. The observed aggregate lateral motion was then introduced into an FEM to simulate the shear stress on the cells (see ESI† S2 for full description of model and analysis).

Acoustic streaming characterization

Streaming flow velocities were measured using particle image velocimetry (PIV) as described in Zmijan et al.[70] 1 µm fluorescent polystyrene beads were used as tracers, imaging with a 10× objective at 400 ms frame intervals. Image data was analyzed via the MATLAB package MPIV[70] to quantify bead displacement and mean particle velocity between sequential frames. Following particle analysis, the median of each frame's particle velocities was established.

Isolation of human articular chondrocytes

HACs were isolated by sequential enzymatic digestion of deep-zone articular cartilage pieces dissected from the non-load-bearing region of the femoral heads.[71] Human femoral head samples were obtained from haematologically normal osteoarthritic patients (5 male, 7 female, mean age of 65) following routine total hip arthroplasty surgeries. Only tissue that would have been discarded was used in this study with approval of the Southampton and South West Hampshire Research Ethics Committee (Ref. 210/01). Pieces of deep-zone cartilage were dissected from the femoral heads and digested in 500 µg mL^{-1} trypsin-EDTA for 30 minutes at 37 °C and 5% CO_2. The tissue fragments were washed in PBS and incubated in 1 mg mL^{-1} hyaluronidase for 15 minutes at 37 °C and 5% CO_2. The resulting fragments were washed in PBS and then incubated in 10 mg mL^{-1} collagenase B (Roche Diagnostics 11088807001) overnight at 37 °C. The resulting cell suspension was filtered through a 70 µm sieve to remove undigested tissue/debris. Isolated chondrocytes were cultured to confluence in monolayer cultures in α-MEM supplemented with 10% (v/v) FBS, 100 unit per mL penicillin, 100 unit per mL streptomycin, and 100 µM ascorbate 2-phosphate. Cultures were maintained in humidified atmosphere at 37 °C, 5% CO_2 and 21% O_2. Passage 1 cells were utilized for the experiments.

ATDC5 cell culture

To probe the acoustic forces within the resonator (for the results shown in Fig. 2), immortalized murine chondrocytes, ATDC5 (Lonza), were used as a representative cell line. Monolayer cultures of murine chondrogenic ATDC5 cells were cultured in DMEM supplemented with 5% (v/v) FBS and 1× insulin-transferrin-selenium premix (ITS; insulin: 10 µg ml^{-1}; transferrin: 5.5 µg ml^{-1}; selenium: 5 ng ml^{-1}). Cultures were maintained in humidified atmosphere at 37 °C, 5% CO_2 and 21% O_2.

Bioreactor culture of human articular chondrocytes

The bioreactor was sterilized under UV light overnight prior to use. Monolayer cultured HACs were harvested at confluence and suspended in serum-free chondrogenic medium consisting of α-MEM supplemented with transforming growth factor-beta (10 ng mL^{-1}, TGF-β3, Peprotech 100-36E), 1× ITS, dexamethasone (10 nM, D4902), and L-ascorbate-2-phosphate (100 µM, A2P, A8960). Prior to cell insertion into the resonators, 9 mL of chondrogenic media was introduced into the bioreactor chamber, thereby fully immersing the resonators. Trapped air bubbles within the fluid layers of the

resonators were removed and the function generator driving the bioreactor was enabled prior to any cell introduction into the resonators. Considering that the fluid layer dimensions are 10 mm × 12 mm × 0.55 mm (occluding volume then being 66 µL), 1.1×10^6 cells were suspended in 50 µl of chondrogenic media and introduced directly into the fluid layer of each resonator using a flexible gel-loading pipette tip, and cultured within the acoustic trap for 21 days under hypoxic conditions (37 °C, 5% CO_2 and 5% O_2). The media in the bioreactor was exchanged with fresh chondrogenic media every 2–3 days under sterile conditions in a tissue culture hood. To aid the transfer between the tissue culture hood and incubator, whilst continuously levitating the cells, the function generator was temporarily switched from a 12 V DC power supply to a battery as a portable power source.

The bioreactor was driven with a sweep range of 200 kHz (centered on the average experimentally derived cavity resonance for the bioreactor plate, approximately 1.5 MHz) and 10 V_{pp}, with a sweep rate of either 50 Hz or 2 Hz to investigate how the change in acoustic forces affects chondrogenesis. The 200 kHz bandwidth of the sweep was chosen as follows: It was found that there is a cluster of resonances close to the main levitation frequency, typically around 100 kHz in bandwidth. Beyond this little acoustic activity is typically observed. The wider 200 kHz bandwidth was chosen such that a similar cluster was visited in each device despite variations between devices. In some cultures, 10 ng mL^{-1} of parathyroid hormone-related protein (PTHrP[1–34], Bachem H-9095) and 30 mM of L-proline (P0380) were added to the chondrogenic medium, which was introduced into the bioreactor from days 10 to 21.

To minimize possible damage and conformational changes to the engineered tissue, the reflector layer was removed and the constructs were extracted from the active region of the resonators. Samples were then either prepared for histological analysis or introduced into an explant of native cartilage for mechanical testing. Preparation for histological staining was accomplished by chemically fixing the tissue overnight at 4 °C with either 90% ethanol or 4% paraformaldehyde (PFA).

Mechanical testing of cartilage explants

In order to assess the mechanical properties of the engineered tissue, the constructs were implanted into native cartilage and cultured for six weeks prior to nano-indentation. Full-thickness cartilage explants were harvested from the non-load bearing regions of osteoarthritic femoral heads and a defect was created in the explant using a 3 mm ball-drill bit. The engineered cartilage was positioned into the defect and the model was cultured on a transwell insert for six weeks at 37 °C and 5% CO_2.

Following the culture period, nanoindentation testing was performed using a NanoTest Vantage System (Micro Materials, Wrexham, UK), using a 400 µm diameter, diamond cono-spherical tip (E_i/Young's modulus = 1141 GPa, v_i/Poisson's ratio = 0.07) in the liquid cell attachment to ensure the samples were submerged in PBS and stayed fully hydrated.

The indentation points were manually selected on both the native cartilage and the engineered tissue. The indentations were run in load control to a maximum load of 0.05 mN at a rate of 0.005 mN s^{-1} with a dwell at peak load of 60 s to allow for creep run out. The average indentation depth was 2.5 µm ± 0.39 µm, which is less than 5% of the original material thickness of 2 mm to ensure the mechanics were reflective of the construct without any substrate influence.[62]

The data acquired from three indentation points was used to determine the mean reduced moduli (E_r) of the engineered and native cartilage and repeated for three patients. In order to obtain the Young's modulus (E_s) from the reduced modulus output by the nano-indentor, the Poisson's ratio (v_s) of both the native and engineered cartilage was assumed to be 0.34.[49–51] The Young's modulus was then calculated by rearranging the terms from the general indenter equation[72] (eqn (1)).

$$E_s = \frac{(E_r E_i)(1 - v_s^{\,2})}{E_i - E_r(1 - v_i^{\,2})} \tag{1}$$

Histology

Paraffin embedding and sectioning. Fixed samples were washed in PBS before processing through graded ethanol (50–100%), followed by clearing with Histoclear (National Diagnostics HS-200). The tissue samples were then embedded in paraffin wax (Fisher 8002-74-2). Sequential sections were cut 7 µm thick on the microtome and mounted on glass slides.

For histological and immunohistochemical staining, paraffin sections were de-waxed and rehydrated through Histoclear, followed by graded ethanol (100–50%).

Alcian blue/Sirius red (A/S) staining. Sections were stained with Alcian blue 8GX (5 mg ml^{-1} in 1% (v/v) glacial acetic acid) and Sirius red F3B (10 mg ml^{-1} in saturated picric acid) following nuclear staining with Weigert's haematoxylin, as described previously.[73] Alcian blue stained the proteoglycan-rich cartilage matrix, while Sirius red stained the collagen-rich matrix.

Immunohistochemistry (IHC) staining. After de-paraffinization and rehydration, sections were quenched of endogenous peroxidase activity with 3% (v/v) H_2O_2 for five minutes at room temperature and blocked with 1% BSA in PBS for five minutes at 4 °C. Sections were incubated with relevant primary antiserum at 4 °C overnight. This was followed by three five minute washes in wash buffer (0.5% Tween 20 in PBS). Slides were then incubated for one hour with the appropriate biotinylated secondary antibody (dilution 1:100), washed three times for five minutes and then incubated for thirty minutes with ExtrAvidin–peroxidase (dilution 1:50). Visualisation of the immune complex involved the avidin-biotin method linked to peroxidase and AEC (3-amino-9-ethylcarbazole), resulting in a reddish brown reaction product following ten minute exposure to 30% peroxide. Negative controls (omission of the primary antisera) were included in all immunohistochemistry procedures. No staining

was observed in any negative control sections. All sections were counter-stained with Alcian Blue 8GX. Glass coverslips were mounted with Hydromount (National Diagnostics) and allowed to dry for at least two hours.

The anti-SOX-9 antibody (rabbit polyclonal, IgG, Millipore, Watford, UK) was used at a dilution of 1 : 150 in 1% BSA in PBS following the antigen retrieval procedure, which involved treating sections in 0.01 M citrate buffer (pH 6.0) for thirty minutes at 75 °C before the application of the standard immunohistochemistry procedure.

For immunostaining using anti-collagen Type I, II and X antibodies as well as the anti-osteopontin (OPN) antibody, sections were treated with Hyaluronidase (0.8 mg ml^{-1}) at 37 °C for 20 minutes in order to unmask the epitopes and render them accessible for immunostaining. The LF68 anti-collagen Type I antibody (COLI rabbit IgG, gift from Dr Larry Fisher), anti-collagen Type II antibody (COLII rabbit IgG, Calbiochem, Watford, UK), anti-collagen Type X antibody (COLX rabbit IgG, Calbiochem, Watford, UK), and anti-OPN antibody (rabbit IgG, GeneTex Inc.) were used at a dilution of 1 : 1000, 1 : 500, 1 : 100, and 1 : 100, respectively.

Alkaline phosphatase staining. Sections, fixed using 90% ethanol, were immersed in activation buffer (Tris Maleate buffer, pH 7.4) overnight at room temperature. The slides were washed prior to interaction with Naphthol AS-B1 phosphate and the diazonium salt (fast red), which was precipitated at the site of the enzyme activity. The slides were mounted as described above.

Image analysis

Histology images were analysed for collagen and proteoglycan staining area by colour-segmentation using k-means cluster analysis. The source image was converted from RGB to L*a*b colour space. The colour information for the tissue section was then isolated from the image by focusing on the information in the a*b colour space. K-means clustering was then used to statistically analyse the mean pixel intensities and partition the pixel locations and values into three clusters (k = 3). This process was replicated three times to minimize cluster overlap.

The algorithm segmented the pixels values such that two clusters contained the pixel colour values on opposite ends of the A*B colour spectrum. For an immunohistochemistry image, the algorithm partitioned the counter-staining (*i.e.* Alcian blue) and target staining (*i.e.* AEC staining) into two clusters. A third cluster contained the intermediary values within the spectrum. Correspondingly, for A/S staining, the algorithm grouped the pixel values according to the Alcian blue target staining cluster, Sirius red staining cluster, and intermediate values cluster. The target staining area was isolated from the target and intermediate value clusters. The background, or whole section area, was segmented by global thresholding by Otsu and morphological filtering was applied to fill any holes within the subsequent binary image of the whole section.

The computed staining area was then normalized to the total section area to give an area fraction.

Microscopy

Histological sections were imaged using Olympus BX 51 dotSlide virtual slide microscope system (Olympus Microscopy). Fluorescence time-lapse images were obtained using an Olympus upright fluorescence microscope with FITC filter (excitation/emission wavelengths: 485 nm/515 nm, Carl Zeiss), Rhodamine filter (excitation/emission wavelengths: 546 nm/560 nm, Carl Zeiss), and Orca-Flash4.0 (Hammamatsu) with HCImage software.

Author contributions

Conflicts of interest

The authors declare no competing financial interests.

Acknowledgements

References

1 A. M. Bhosale and J. B. Richardson, *Br. Med. Bull.*, 2008, **87**, 77–95.
2 S. N. Redman, S. F. Oldfield and C. W. Archer, *Eur. Cells Mater.*, 2005, **9**, 23–32.
3 R. M. Schek, J. M. Taboas, S. J. Segvich, S. J. Hollister and P. H. Krebsbach, *Tissue Eng.*, 2004, **10**, 1376–1385.
4 A. Khademhosseini, R. Langer, J. Borenstein and J. P. Vacanti, *Proc. Natl. Acad. Sci. U. S. A.*, 2006, **103**, 2480–2487.
5 R. Langer and J. Vacanti, *Science*, 1993, **260**, 920–926.
6 H. Da, S. J. Jia, G. L. Meng, J. H. Cheng, W. Zhou, Z. Xiong, Y. J. Mu and J. Liu, *PLoS One*, 2013, **8**, e54838.
7 D. Tang, R. S. Tare, L. Y. Yang, D. F. Williams, K. L. Ou and R. O. Oreffo, *Biomaterials*, 2016, **83**, 363–382.

8 D. M. Gibbs, C. R. Black, J. I. Dawson and R. O. Oreffo, *J. Tissue Eng. Regener. Med.*, 2016, **10**, 187–198.

9 C. R. Black, V. Goriainov, D. Gibbs, J. Kanczler, R. S. Tare and R. O. Oreffo, *Curr. Mol. Biol. Rep.*, 2015, **1**, 132–140.

10 H. W. Kang, S. J. Lee, I. K. Ko, C. Kengla, J. J. Yoo and A. Atala, *Nat. Biotechnol.*, 2016, **34**, 312–319.

11 D. M. Gibbs, C. R. Black, G. Hulsart-Billstrom, P. Shi, E. Scarpa, R. O. Oreffo and J. I. Dawson, *Biomaterials*, 2016, **99**, 16–23.

12 T. Xu, K. W. Binder, M. Z. Albanna, D. Dice, W. Zhao, J. J. Yoo and A. Atala, *Biofabrication*, 2013, **5**, 015001.

13 K. Y. Ching, O. G. Andriotis, S. Li, P. Basnett, B. Su, I. Roy, R. S. Tare, B. G. Sengers and M. Stolz, *J. Biomater. Appl.*, 2016, 0885328216639749.

14 S. Li, P. Glynne-Jones, O. G. Andriotis, K. Y. Ching, U. S. Jonnalagadda, R. O. Oreffo, M. Hill and R. S. Tare, *Lab Chip*, 2014, **14**, 4475–4485.

15 S. Li, B. G. Sengers, R. O. Oreffo and R. S. Tare, *J. Biomater. Appl.*, 2015, **29**, 824–836.

16 J. C. Babister, R. S. Tare, D. W. Green, S. Inglis, S. Mann and R. O. Oreffo, *Biomaterials*, 2008, **29**, 58–65.

17 R. S. Tare, D. Howard, J. C. Pound, H. I. Roach and R. O. Oreffo, *Biochem. Biophys. Res. Commun.*, 2005, **333**, 609–621.

18 I. T. Ozbolat and Y. Yu, *IEEE Trans. Biomed. Eng.*, 2013, **60**, 691–699.

19 K. C. Hribar, P. Soman, J. Warner, P. Chung and S. Chen, *Lab Chip*, 2014, **14**, 268–275.

20 M. Vaezi and S. Yang, *Int. J. Bioprint.*, 2015, **1**, 66–76.

21 M.-H. Wu, H.-Y. Wang, C.-L. Tai, Y.-H. Chang, Y.-M. Chen, S.-B. Huang, T.-K. Chiu, T.-C. Yang and S.-S. Wang, *Sens. Actuators, B*, 2013, **176**, 86–96.

22 B. Labbe, G. Marceau-Fortier and J. Fradette, *Methods Mol. Biol.*, 2011, **702**, 429–441.

23 M. Sato, M. Yamato, K. Hamahashi, T. Okano and J. Mochida, *Anat. Rec.*, 2014, **297**, 36–43.

24 S. P. Nukavarapu and D. L. Dorcemus, *Biotechnol. Adv.*, 2013, **31**, 706–721.

25 G. Vunjak-Novakovic, I. Martin, B. Obradovic, S. Treppo, A. J. Grodzinsky, R. Langer and L. E. Freed, *J. Orthop. Res.*, 2016, **17**, 130–138.

26 A. J. Grodzinsky, M. E. Levenston, M. Jin and E. H. Frank, *Annu. Rev. Biomed. Eng.*, 2003, **2**, 691–713.

27 H. Ogawa, E. Kozhemyakina, H.-H. Hung, A. J. Grodzinsky and A. B. Lassar, *Genes Dev.*, 2014, **28**, 127–139.

28 J. Fischer, A. Dickhut, M. Rickert and W. Richter, *Arthritis Rheum.*, 2010, **62**, 2696–2706.

29 Y. J. Kim, H. J. Kim and G. I. Im, *Biochem. Biophys. Res. Commun.*, 2008, **373**, 104–108.

30 T. Xu, K. Yang, H. You, A. Chen, J. Wang, K. Xu, C. Gong, J. Shao, Z. Ma and F. Guo, *Bone*, 2013, **56**, 304–311.

31 D. Bazou, A. Castro and M. Hoyos, *Ultrasonics*, 2012, **52**, 842–850.

32 K. A. Garvin, D. Dalecki, M. Yousefhussien, M. Helguera and D. C. Hocking, *J. Acoust. Soc. Am.*, 2013, **134**, 1483–1490.

33 K. A. Garvin, D. C. Hocking and D. Dalecki, *Ultrasound Med. Biol.*, 2010, **36**, 1919–1932.

34 K. A. Garvin, J. VanderBurgh, D. C. Hocking and D. Dalecki, *J. Acoust. Soc. Am.*, 2013, **134**, 1491–1502.

35 A. L. Bernassau, F. Gesellchen, P. G. A. MacPherson, M. Riehle and D. R. S. Cumming, *Biomed. Microdevices*, 2012, **14**, 559–564.

36 X. Ding, J. Shi, S.-C. S. Lin, S. Yazdi, B. Kiraly and T. J. Huang, *Lab Chip*, 2012, **12**, 2491–2497.

37 F. Guo, Z. Mao, Y. Chen, Z. Xie, J. P. Lata, P. Li, L. Ren, J. Liu, J. Yang, M. Dao, S. Suresh and T. J. Huang, *Proc. Natl. Acad. Sci. U. S. A.*, 2016, **113**, 1522–1527.

38 D. J. Collins, B. Morahan, J. Garcia-Bustos, C. Doerig, M. Plebanski and A. Neild, *Nat. Commun.*, 2015, **6**, 8686.

39 J. Liu, L. A. Kuznetsova, G. O. Edwards, J. Xu, M. Ma, W. M. Purcell, S. K. Jackson and W. T. Coakley, *J. Cell. Biochem.*, 2007, **102**, 1180–1189.

40 C. Bouyer, P. Chen, S. Guven, T. T. Demirtas, T. J. Nieland, F. Padilla and U. Demirci, *Adv. Mater.*, 2016, **28**, 161–167.

41 A. Lenshof, C. Magnusson and T. Laurell, *Lab Chip*, 2012, **12**, 1210–1223.

42 P. Glynne-Jones, C. Démoré, C. Ye, Y. Qiu, S. Cochran and M. Hill, *IEEE Trans. Ultrason. Ferroelectr. Freq. Control*, 2012, **59**, 1258–1266.

43 L. A. Crum, *J. Acoust. Soc. Am.*, 1975, **57**, 1363–1370.

44 G. O. Edwards, W. T. Coakley, J. R. Ralphs and C. W. Archer, *Eur. Cells Mater.*, 2010, **19**, 1–12.

45 A. Garbin, I. Leibacher, P. Hahn, H. Le Ferrand, A. Studart and J. Dual, *J. Acoust. Soc. Am.*, 2015, **138**, 2759–2769.

46 S. Li, R. O. Oreffo, B. G. Sengers and R. S. Tare, *Biotechnol. Bioeng.*, 2014, **111**, 1876–1885.

47 S. Oberti, A. Neild, R. Quach and J. Dual, *Ultrasonics*, 2009, **49**, 47–52.

48 M. Wiklund, A. Christakou, M. Ohlin, I. Iranmanesh, T. Frisk, B. Vanherberghen and B. Önfelt, *Micromachines*, 2014, **5**, 27–49.

49 A. E. Christakou, M. Ohlin, B. Onfelt and M. Wiklund, *Lab Chip*, 2015, **15**, 3222–3231.

50 O. Manneberg, B. Vanherberghen, B. Onfelt and M. Wiklund, *Lab Chip*, 2009, **9**, 833–837.

51 D. Bazou, R. Kearney, F. Mansergh, C. Bourdon, J. Farrar and M. Wride, *Ultrasound Med. Biol.*, 2011, **37**, 321–330.

52 S. J. Wang, D. Jiang, Z. Z. Zhang, A. B. Huang, Y. S. Qi, H. J. Wang, J. Y. Zhang and J. K. Yu, *Sci. Rep.*, 2016, **6**, 36400.

53 J. Fischer, A. Aulmann, V. Dexheimer, T. Grossner and W. Richter, *Stem Cells Dev.*, 2014, **23**, 2513–2523.

54 S. S. Sadhal, *Lab Chip*, 2012, **12**, 2292–2300.

55 M. Wiklund, R. Green and M. Ohlin, *Lab Chip*, 2012, **12**, 2438–2451.

56 J. Lei, P. Glynne-Jones and M. Hill, *Lab Chip*, 2013, **13**, 2133–2143.

57 J. Lei, P. Glynne-Jones and M. Hill, *Phys. Fluids*, 2016, **28**, 012004.

58 P. B. Muller and H. Bruus, *Phys. Rev. E: Stat., Nonlinear, Soft Matter Phys.*, 2015, **92**, 063018.

59 B. Khozoee, P. Mafi, R. Mafi and W. S. Khan, *Curr. Stem Cell Res. Ther.*, 2017, **12**, 260–270.

60 C. Bandeiras and A. Completo, *Biomech. Model. Mechanobiol.*, 2017, **16**, 651–666.

61 C. H. Fung, W. H. Cheung, N. M. Pounder, F. J. de Ana, A. Harrison and K. S. Leung, *Ultrasonics*, 2014, **54**, 850–859.

62 N. P. Whitney, A. C. Lamb, T. M. Louw and A. Subramanian, *Ultrasound Med. Biol.*, 2012, **38**, 1734–1743.

63 X. Chen, F. He, D. Y. Zhong and Z.-P. Luo, *BioMed Res. Int.*, 2015, **2015**, 1–10.

64 M. Evander, L. Johansson, T. Lilliehorn, J. Piskur, M. Lindvall, S. Johansson, M. Almqvist, T. Laurell and J. Nilsson, *Anal. Chem.*, 2007, **79**, 2984–2991.

65 M. Wiklund, *Lab Chip*, 2012, **12**, 2018–2028.

66 O. R. Schatti, L. M. Gallo and P. A. Torzilli, *Ann. Biomed. Eng.*, 2015, **44**, 2577–2588.

67 M. Hill, Y. Shen and J. J. Hawkes, *Ultrasonics*, 2002, **40**, 385–392.

68 S. P. Martin, R. J. Townsend, L. A. Kuznetsova, K. A. J. Borthwick, M. Hill, M. B. McDonnell and W. T. Coakley, *Biosens. Bioelectron.*, 2005, **21**, 758–767.

69 L. P. Gor'kov, *Soviet Physics-Doklady*, 1962, **6**, 773–775.

70 R. Zmijan, U. S. Jonnalagadda, D. Carugo, Y. Kochi, E. Lemm, G. Packham, M. Hill and P. Glynne-Jones, *RSC Adv.*, 2015, **5**, 83206–83216.

71 M. C. de Andres, K. Imagawa, K. Hashimoto, A. Gonzalez, M. B. Goldring, H. I. Roach and R. O. Oreffo, *Biochem. Biophys. Res. Commun.*, 2011, **407**, 54–59.

72 W. C. Oliver and G. M. Pharr, *J. Mater. Res.*, 2004, **19**, 3–20.

73 L. Lison, *Stain Technol.*, 1954, **29**, 131–138.